Acta Geotechnica (2014) 9:499–511
DOI 10.1007/s11440-013-0285-9

RESEARCH PAPER

Numerical analysis of a pile–slab-supported railway embankment

Yan Jiang · Jie Han · Gang Zheng

Received: 7 October 2012 / Accepted: 9 October 2013 / Published online: 11 December 2013

Abstract This paper presents a numerical analysis of a well-monitored pile–slab-supported embankment for the Beijing–Tianjin high-speed railway in China. Cement–fly ash–gravel piles were used in this project. A coupled two-dimensional mechanical and hydraulic numerical model was used for this analysis and the results are compared with the field measurements including settlement, load distribution between soil and pile, and excess pore pressure. The numerical model calculated the settlement profile close to that measured in the field. The proportion of the load carried by the soil was small thus significantly reducing the settlement. The stress transfer from the soil to the piles reduced the excess pore pressure effectively. A parametric study was conducted to investigate the influence of three key factors on the performance of the embankment. The parametric study indicated that the existence of a cushion reduced the shear force in the slab. The increase in slab thickness and pile stiffness increased the shear force and bending moment in the slab. An increase in pile stiffness reduced the settlement and lateral displacement of the embankment.

Keywords Embankment · Load transfer · Numerical analysis · Pile · Settlement

Y. Jiang · J. Han (✉)
Department of Civil, Environmental and Architectural Engineering (CEAE), The University of Kansas, Lawrence, KS 66045, USA
e-mail: jiehan@ku.edu

G. Zheng
Department of Civil Engineering, Tianjin University, Tianjin 300072, China

1 Introduction

The Beijing–Tianjin high-speed railway is located in north China and connects two large cities—Beijing and Tianjin as shown in Fig. 1. The length of this railway is 115 km and the design speed of high-speed strains is 350 km/h. A portion of the railway was constructed on embankments. Engineers faced major challenges in designing high-speed railway embankments on soft soil, which has low bearing capacity and large potential total and differential settlements. To mitigate these potential problems, ground improvement techniques are necessary. The possible techniques include fill and/or vacuum preloading, vertical drainage, overexcavation and replacement, stone columns, deep mixed columns, rigid piles. [29].

Pile (or column)-supported embankments, as a rapid construction technique, have been increasingly adopted to increase the bearing capacity and reduce the total and differential settlements. Piles under the embankment are usually installed through soft soil layers to transfer the embankment and traffic loads to deep and firm strata.

When piles are used, pile caps are often adopted to reduce clear spacing of piles, transfer more embankment load to the piles, and reduce differential settlement between pile caps [16, 19, 28]. To minimize the differential settlement between pile caps, one or multiple geosynthetic layers can be placed above the pile caps as a horizontal reinforcement. This embankment system is referred as the geosynthetic-reinforced pile-supported (GRPS) embankment [16, 22]. Han and Gabr [15] found that the coverage of pile caps for GRPS embankments is typically 10–20 % as compared to 50–70 % for conventional pile-supported embankments without a geosynthetic.

In the past few years, GRPS embankments have been increasingly adopted and researched. For instance, Han and

Fig. 1 Map showing the high-speed railway from Tianjin (A) to Beijing (B) (*Source* Google Earth)

Gabr [15], Huang et al. [19], Jenck et al. [23], Smith and Filz [33], Abusharar et al. [1], Huang et al. [22], Huang and Han [21], Jenck et al. [24], Huang and Han [20], and Han et al. [14] conducted two-dimensional or three-dimensional numerical analyses to investigate the load transfer mechanisms, differential settlements between piles, and/or consolidation behavior of GRPS embankments. The load transfer mechanisms above the pile caps involve soil arching within the embankment fill and tensioned membrane of the geosynthetic layer. Chen et al. [8] conducted model tests to investigate the soil arching mechanism in embankments with and without reinforcement. Hironaka et al. [18] investigated the soil arching modes using the advanced computed tomography technology. Due to the higher stiffness of the piles, the consolidation of the foundation is much accelerated [22]. Wang et al. [38] conducted a numerical analysis on a similar application dealing with geosynthetic-bridged and drilled shaft-supported embankments over large sinkhole. A number of field studies were reported on the use of GRPS embankments, such as Card and Carter [6], Alzamora et al. [2], Han and Akins [13], Zanziger and Gartung [39], and Liu et al. [28]. These field studies verified the load transfer mechanisms, the development of differential settlement between piles, and the consolidation behavior of GRPS embankments. Collin [11] provided a state-of-the-practice review of load transfer platforms in column-supported embankments. Several theories were proposed by different researchers to analyze effects of soil arching and tensioned membrane in piled embankments. For instance, Hewlett and Randolph [17] and Kempfert et al. [25] proposed soil arching theories based on the vault shape models. Carlsson [7], Card and Carter [6], Miki [30], and Svano et al. [35] proposed soil wedge models to simulate soil arching in the embankment fill supported by piles. The British Standard BS8006 [4] adopted Marston's formula for positive projecting subsurface conduits to calculate the average vertical stress on the pile caps. Russell and Pierpoint [32] assessed an approach based on the Terzaghi soil arching theory, which considered the equilibrium of the soil zones above the soft soil. Chen et al. [9] assumed one-dimensional compression of the pile, the embankment fill, and the foundation soil and obtained the solutions for the embankment settlement, the skin friction along the pile shaft, and the proportion of the load carried by the piles. However, Stewart and Filz [34] found that the design methods based on different soil arching models resulted in very different vertical stresses above the geosynthetic. The tensioned membrane theories included in the British Standard BS 8006 [4] and Giroud et al. [12] have

been commonly used to estimate the tension in the geosynthetic layer. In summary, the GRPS system transfers most of the embankment load through soil arching and tensioned membrane to the piles. A number of studies have been conducted to investigate the mechanisms and develop the solutions for this load transfer.

However, GRPS embankments may still have relatively larger total and differential settlements than the requirements for high-speed railways. Under such a condition, a concrete slab may be adopted to replace the geosynthetic layer in the embankment design to offer stronger reinforcement and reduce total and differential settlements. Herein, this embankment is called a pile–slab-supported (PSS) embankment to differentiate it from the GRPS embankment. The PSS embankment was used for the Beijing–Tianjin high-speed railway. A field study was conducted to evaluate the performance of this embankment. Since the PSS embankment has a different structure, it is expected to have different performance from the GRPS embankment. The obvious difference is that the concrete slab is relatively rigid so that small differential settlement will develop in the embankment. In other words, the soil arching effect can be neglected for the PSS embankment. Under such a condition, most of the embankment and traffic loads will be applied on the piles through the rigid slab; therefore, the slab is expected to play an important role in the purpose of reducing total settlement, differential settlement, and lateral displacement of the embankment. However, limited studies have been conducted on the PSS embankment. Therefore, to better understand the performance of the PSS embankment, a field study and numerical analysis were conducted.

In the field study, settlements, excess pore water pressure, and earth pressure during the embankment construction were monitored with time for approximately 450 days. Details of the field study and results were reported in Zheng et al. [40], but a brief description will be presented later for comparison purposes. This paper focuses on the numerical analysis of an instrumented PSS embankment along the Beijing–Tianjin high-speed railway. The two-dimensional finite element method incorporated in the commercial software Abaqus was adopted for the numerical analysis. The numerical analysis simulated the consolidation of the PSS embankment by a coupled mechanical and hydraulic model. The rows of piles parallel to the centerline of the embankment were modeled as pile walls. Tan et al. [36] clearly demonstrated that two-dimensional numerical models with pile walls can well simulate the generation and dissipation of excess pore water pressure in the stone-column-reinforced soft foundation under the embankment as compared to the three-dimensional numerical model. In addition, a parametric study was conducted to investigate three key influence factors on the performance of the PSS embankment including slab thickness, cushion, and pile stiffness.

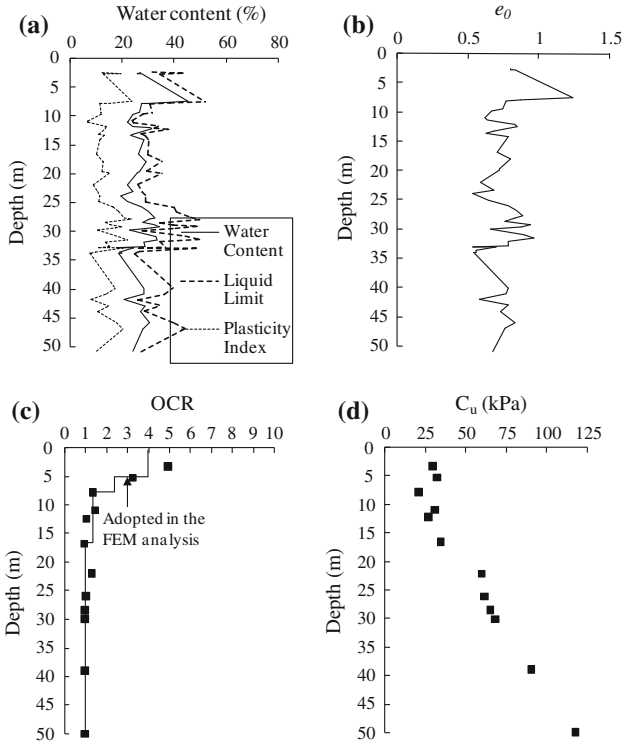

Fig. 2 Soil profiles (modified from Zheng et al. [40])

2 Site conditions and soil properties

The high-speed railway embankment in this study was located at Station DK84+150 between the Yangcun Bridge and the Yongding River Bridge within the Wuqing district of Tianjin, China. The project site mainly consisted of inter-layered marine and continental deposits. The soil profile at this station was a 5.2-m-thick medium clay underlain by a 2.8-m-thick soft clay and a 42-m-thick medium to stiff clay. Figure 2 presents the soil properties, which include natural water content, liquid limit, plasticity index, initial void ratio, over consolidation ratio (OCR), and undrained shear strength. The water contents and liquid limits are the average profiles generated based on laboratory data of soil samples from field. The plasticity index profile was calculated by the relationship $I_p = w_l - w_p$ where w_l and w_p were liquid limit and plasticity limit, respectively. The OCR values were determined by oedometer tests. The OCR profile adopted for the numerical study was estimated by the average of the OCR data available for the same layer of soil. The soil's undrained shear strength was estimated using the formula $c_u = 0.25\sigma'_v(\mathrm{OCR})^{0.8}$ proposed by Ladd et al. [27]. The

Table 1 Average soil properties [40]

Soil layer	Thickness (m)	Unit weight (kN/m^3)	Water content (%)	Liquid limit (%)	Plastic limit (%)	Void ratio	Constrained modulus (MPa)
Medium clay	5.2	19.1	27.2	32.8	20.4	0.8	12.25
Soft clay	2.8	18	41.9	48	26.8	1.2	5.95
Medium to stiff clay	32	19.4	26.4	33.7	20.2	0.73	11.30

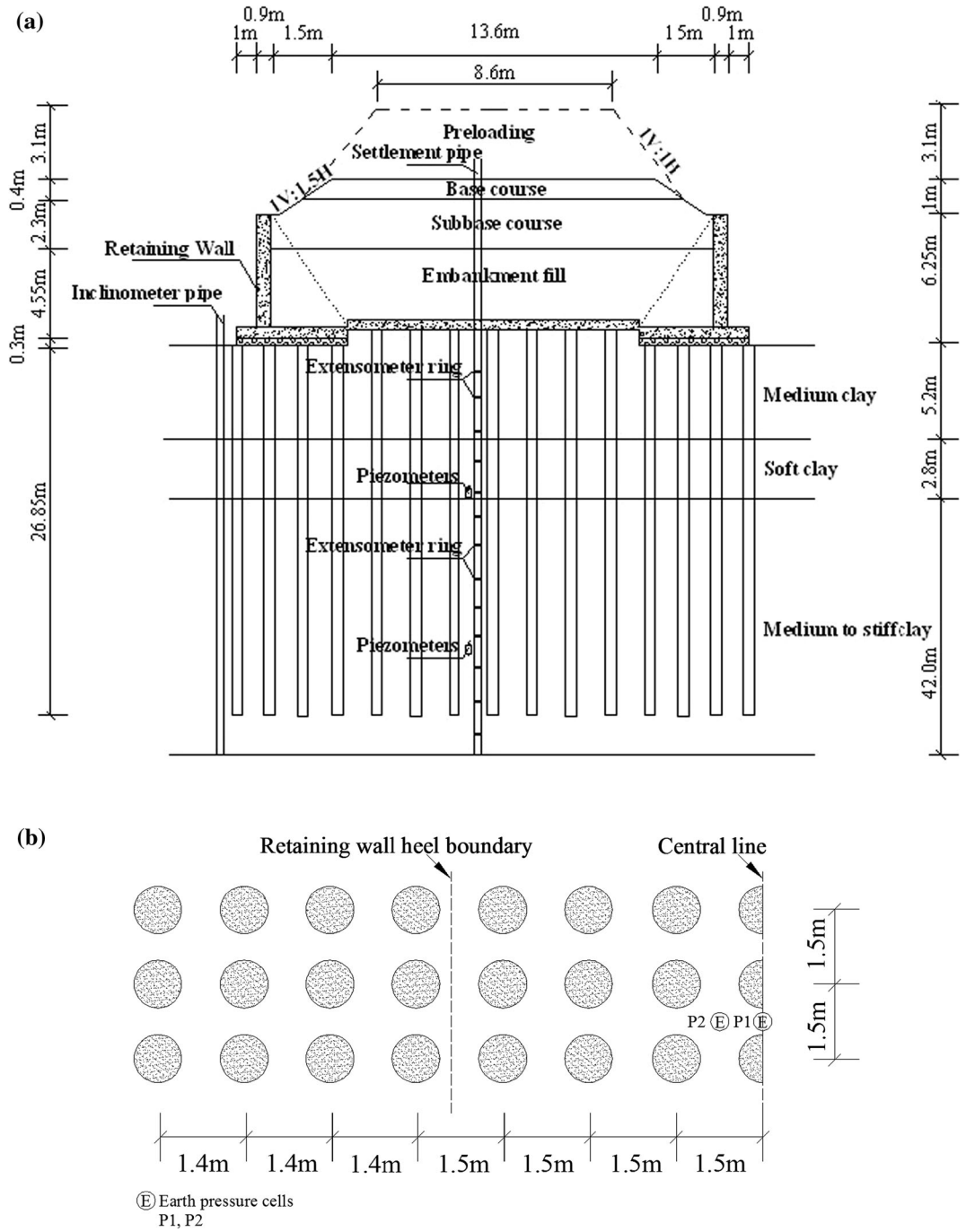

Fig. 3 Cross-sectional and plan views of the PSS embankment and locations of instrumentations: a cross-sectional view of the instrumented embankment (not to scale) and b plan view (not to scale) (modified from Zheng et al. [40])

groundwater table was at 0.6–2.5 m deep below the ground surface. Figure 2 shows that the soil's undrained shear strength increased almost linearly with depth while the OCR values decreased with depth. The solid lines of OCR in Fig. 2 were used for the numerical analysis. According to the Unified Soil Classification System (USCS), the soils in this project site were mostly low plasticity clays. The soil layers listed in Table 1 were defined according to Terzaghi et al. [37]. The average soil properties for each layer are summarized in Table 1. The soil constrained moduli were calculated based on the consolidation data.

3 Pile–slab-supported embankment

Figure 3 shows the cross-sectional and plan views of the PSS railway embankment of 7.25 m high with a 13.6-m-wide crest and 1(V):1.5(H) side slopes. The embankment included 4.55-m-thick embankment fill, 2.3-m-thick subbase course, and 0.4-m-thick base course. The materials of the embankment fill, subbase course, and base course were cement-stabilized soil, well-graded sand and gravel, and well-graded aggregate, respectively. The elastic moduli of these materials were all over 45 MPa. In the numerical analysis, the elastic moduli of the embankment fill and subbase course had limited influence on the results due to the existence of the slab and thus were considered to be same for simplicity. Reinforced concrete counterfort retaining walls were constructed on both sides of the embankment to ensure its stability and the center-to-center spacing between two counterforts along the length of the embankment was 3 m.

A 0.5-m-thick reinforced concrete slab was constructed under the embankment fill. In the middle portion of the embankment, piles were directly covered by the concrete slab. However, underneath the foundation of the retaining wall, a 0.3-m-thick cushion (a 0.1-m-thick low-strength concrete cushion laid on a 0.2-m-thick gravel cushion) was placed on the top of piles. Below the cushions were cement–fly ash–gravel (CFG) piles. These piles were cast-in-place and had unconfined compressive strength higher than 20 MPa. Bruce [5] suggested that a typical correlation between the elastic modulus and the field unconfined compressive strength of the soil treated by cement be $E = (150–500)\ q_u$ where E is the elastic modulus and q_u = unconfined compressive strength. Therefore, the elastic modulus of CFG could be estimated as an average by $350\ q_u = 7{,}000$ MPa. Clearly, this modulus is much higher than that of other column systems (e.g., stone columns, deep mixed columns). As a result, CFG piles are commonly regarded as rigid piles in China. The CFG piles used to support retaining walls were 26.85 m long while those used to support the slab were 27.65 m long. The

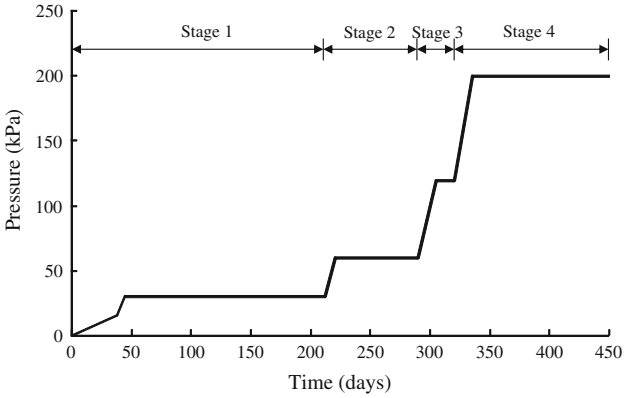

Fig. 4 Embankment load history (modified from Zheng et al. [40])

diameter of the CFG piles was 0.4 m, and they were installed in a square pattern. The center-to-center spacing of CFG piles under the slab and the retaining wall was 1.5 and 1.4 m, respectively, as shown in Fig. 3b. A 3.5-m-high soil surcharge was added on the subbase course for preloading, where a polyester geotextile sheet was laid on the top of the subbase course in order to keep the subbase course separated from the soil surcharge. The soil surcharge at the base had the same width as the top of the subbase course, was compacted to the unit weight higher than 18 kN/m^3, and had a 1(V):1(H) side slope on each side. The base course was added after removing the surcharge when the required consolidation was achieved. Roller compactors were used for compaction of the embankment fill, subbase course, and base course. Figure 4 shows the history of the embankment construction and preloading before the surcharge was removed.

4 Instrumentation

Earth pressure cells, piezometers, and extensometer rings were placed under the concrete slab. The locations of the two earth pressure cells (P1 and P2) are shown in Fig. 3b. The piezometers were placed at depths of 8 and 22 m along the centerline of the embankment. Several magnetic extensometer rings were installed along a plastic pipe close to the centerline of the embankment to measure the settlements below the concrete slab at different depths up to 60 m deep. An inclinometer pipe was installed close to the toe of the retaining wall on the left in Fig. 3a.

5 Numerical modeling

5.1 Model mesh and boundary condition

In the finite element analysis, a two-dimensional plane-strain model was created to simulate the behavior of the

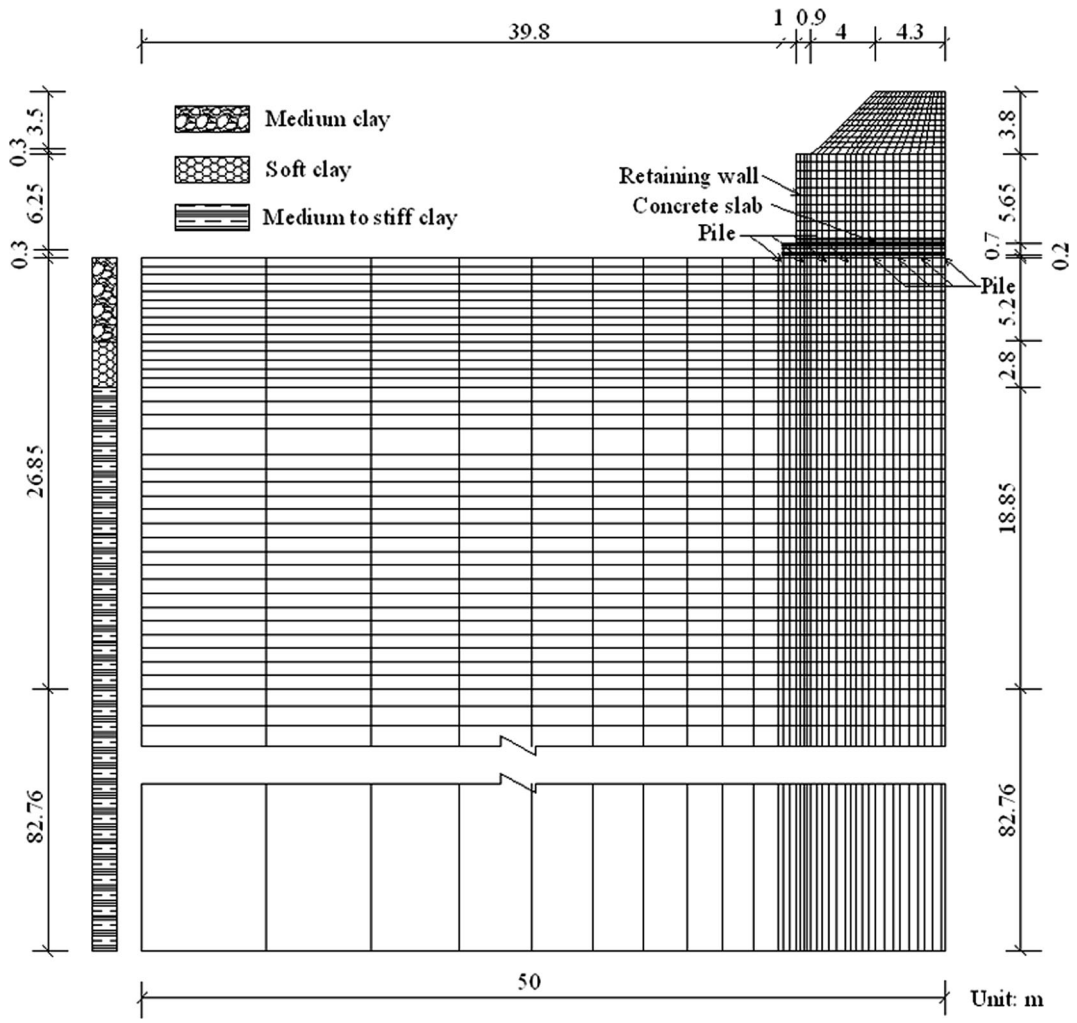

Fig. 5 Model mesh for the finite element analysis

PSS embankment using the commercial finite element software, Abaqus. Due to the symmetry of this embankment, half of the embankment was modeled as shown in Fig. 5 for the finite element mesh. The CFG piles were installed into 26.85 m below the ground surface, but the soil layers were extended to 100 m deep, which is approximately 5 times the width of the embankment. The horizontal distance of the model was 50 m, which is approximately 5 times half-width of the embankment. It is generally believed that when the size of the numerical model is 5 times larger than the loading area, the boundary effect can be ignored. This rule of thumb was verified by Huang et al. [22], in which deep mixed column-supported embankments over soft soil were numerically modeled by mechanical and hydraulic coupling. This approach was also used in this study. Therefore, the influence of the bottom and horizontal boundaries on the numerical results can be ignored. The mechanical boundary conditions were set as follows: on the left and right sides, the horizontal displacements were set to zero while the bottom boundary was fixed in both directions. Water could drain out freely at the ground surface. The left-side boundary was assumed impervious because it is quite far from the centerline of the embankment. The right-side boundary was also set to be impervious because of the symmetry. The bottom of the model was assumed impervious due to the existence of low permeability soil.

5.2 Material properties

The piles, the concrete slab, the retaining wall, and the concrete cushion were modeled as linear elastic materials. The piles arranged in a square pattern are actually a three-dimensional problem. In order to convert the three-dimensional problem into a two-dimensional problem, the equivalent elastic modulus of the pile wall was calculated

Table 2 Soil parameters and properties

Material	Depth (m)	Unit weight (kN/m^3)	e_0	OCR	K_o	ν	λ	κ	M	k × 10^{-4} (m/day)
Medium clay	0–5.2	19.1	0.80	4	1.25	0.3	0.070	0.014	0.86	43.2
Soft clay	5.2–8.0	18	1.20	2.3	0.92	0.3	0.18	0.030	0.9	4.32
Medium to stiff clay	8.0–16.5	19.4	0.73	1.2	0.55	0.3	0.068	0.013	1.19	43.2
	16.5–26.9			1	0.50	0.3	0.045	0.009	1.20	43.2
	26.9–80			1	0.44	0.3	0.015	0.004	1.38	8.64

as follows: $E_{eq} = E_p a_s + E_s(1 - a_s)$ where E_p and E_s are the moduli of pile and soil, respectively; a_s is the area replacement ratio, defined as the ratio of the pile cross-sectional area to the total area. The width of the pile wall was assumed to be equal to the diameter of the pile, and thus, a_s was 0.21 within the pile wall. Considering the soil constraint modulus ranging from 5.95 to 12.25 MPa with an average modulus of 10 MPa (Table 1) and the average modulus of CFG of 7,000 MPa, the equivalent elastic modulus of the pile wall was 1,470 MPa (1,450 MPa used in the analysis).

The embankment fill, the subbase course, the granular cushion, and the preloading soil were modeled as linearly elastic–perfectly plastic materials with Mohr–Coulomb failure envelopes. The soils below the slab were modeled as Modified Cam–Clay (MCC) materials [31]. The MCC model includes five material parameters: slope of swelling line, κ; slope of virgin consolidation line, λ; the initial void ratio, e_0; slope of the critical state line, M; and Poisson's ratio, ν. The values of λ, κ, and e_0 were obtained from one-dimensional consolidation tests. The value of M was obtained from the consolidated undrained triaxial tests with measured pore water pressure. The permeability values of the soils were assumed to be consistent with the empirical values in the Tianjin area, and their values were assumed to be equal in vertical and horizontal directions in the numerical analysis. Coulomb friction was used to simulate the interface between soil and pile. Kulhawy et al. [26] suggested the interface friction coefficient between rough concrete pile and soil range from 0.8tan ϕ to 1.0tan ϕ (ϕ is friction angle of soil). The interface friction coefficient of $\mu = 0.8\tan\phi$ was selected in this study. The Poisson's ratios of concrete and soils were assumed to be 0.2 and 0.3, respectively. The properties of all the materials used in the numerical model are provided in Tables 2 and 3. Four-node plane-strain quadrilateral elements with bilinear displacement and bilinear pore pressure were used for the soils in the ground (i.e., medium clay, soft clay, and medium to stiff clay) while four-node bilinear plane-strain quadrilateral elements were used for other materials. The coupled mechanical and hydraulic modeling follows the quasi-static Biot theory [3].

Table 3 Other parameters and properties

Material	Unit weight (kN/m^3)	E (MPa)	ν	c′ (kPa)	ϕ′	ψ′
Pile	25	1,450	0.2			
Concrete slab	25	20,000	0.2			
Retaining wall	25	20,000	0.2			
Concrete cushion	25	15,000	0.2			
Granular cushion	20	45	0.3	10	40	0
Preloading soil	20	30	0.3	5	30	0
Embankment fill and subbase course	20	45	0.3	10	40	0

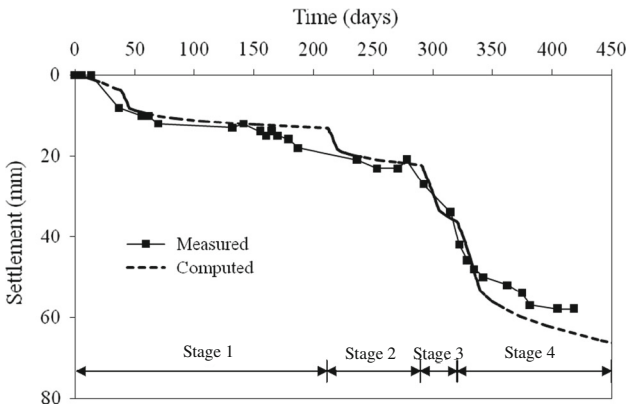

Fig. 6 Measured and computed settlements versus time

6 Numerical results and comparisons

6.1 Settlement

Figure 6 shows the measured and computed settlements with the elapsed time at the base of the embankment near the centerline. It is shown that the computed results agree reasonably well with the measured data. The high settlement rates from 280 to 330 days corresponded to the high embankment filling rate as shown in Fig. 4. However, these settlement rates (less than 2 mm/day) were much less than the requirement of 10 mm/day for this project based on the Chinese Technical Code for Ground Treatment for

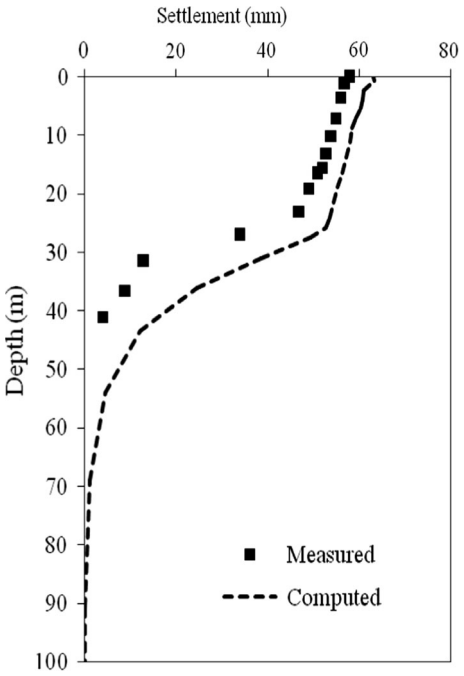

Fig. 7 Measured and computed settlements with depth

Buildings (JGJ 79-2002) [10]. Based on the minimum soil's undrained shear strength ($C_u = 22$ kPa) in the profile (Fig. 2), the maximum embankment height on the natural soil under an undrained condition would be approximately 5.7 m. Obviously, the constructed embankment (more than 7.2 m high) was higher than this maximum embankment height without any ground improvement. This result demonstrated the effectiveness of the rigid CFG piles to increase the bearing capacity of the foundation.

Figure 7 shows the settlement versus depth profile at 2 months after preloading (i.e., the 404th day from the beginning of the construction). The computed settlement captured the overall trend but slightly overestimated the magnitude.

6.2 Vertical stress on soil

Figure 8 presents the measured and computed vertical stresses carried by the soil between piles close to the centerline of the embankment. It is shown that the computed vertical stress followed the general trend of variations, but under-predicted the values as compared to the measured vertical stresses carried by the soil. The computed vertical stresses corresponding to P2 were plotted. Since P1 was on the pile wall in the two-dimensional numerical analysis, the computed vertical stresses would be different from those measured on the pile head. The low stress level (less than 25 kPa) on the soil below the slab demonstrates that majority of the load was carried by the

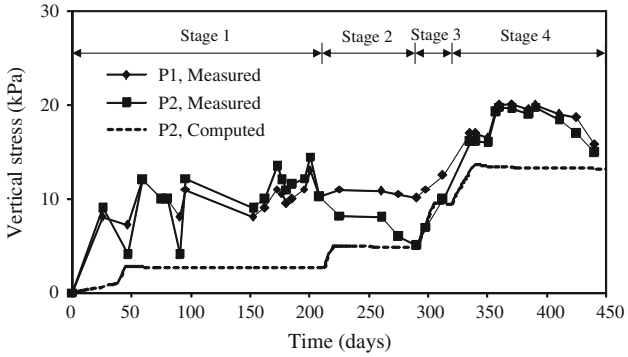

Fig. 8 Measured and computed vertical stresses carried by the soil between piles

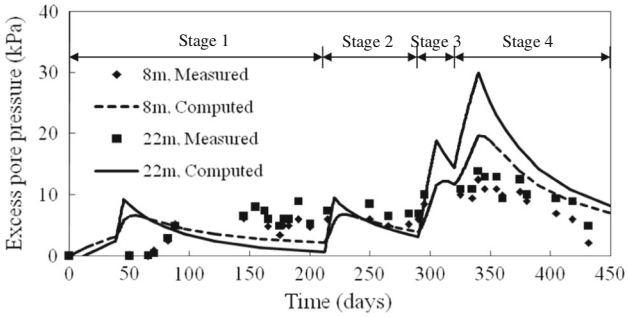

Fig. 9 Measured and computed excess pore water pressures with time

CFG piles. Figure 8 also shows that both the measured and computed vertical stresses on the soil after loading decreased with time. This phenomenon indicates more stress transferred from the soil to the piles. This stress transfer accelerated the consolidation of the soil as pointed out by Han and Ye [16].

6.3 Excess pore water pressure

Figure 9 presents the measured and computed excess pore water pressures with time at depths of 8 and 22 m. It is shown that there was an increase in the excess pore water pressure after each loading and then followed by a dissipation of pore water pressure during the constant load period. The computed pore water pressure from the numerical analysis agreed reasonably well with the measured data at the depth of 8 m, but there was obvious difference between the numerical and measured results at the depth of 22 m. The reason for this difference is unknown. Figure 9 shows that the excess pore water pressures measured and computed at the depth of 22 m were higher than those at the depth of 8 m. This phenomenon can be explained that the piezometer at the depth of 22 m was close to the tip of the piles, and more load was transferred to the pile tips through the rigid CFG piles. The remaining

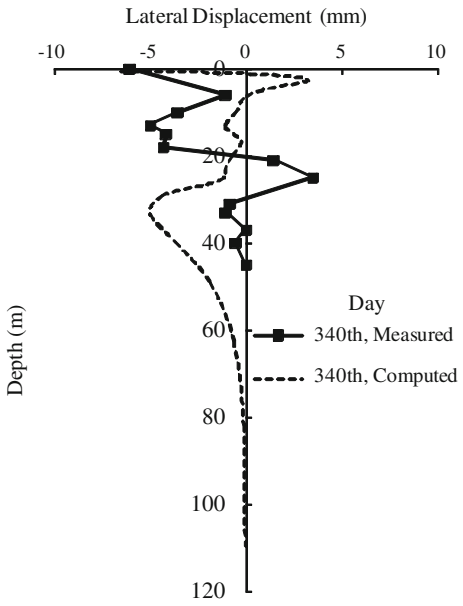

Fig. 10 Measured and computed lateral displacements with depth

excess pore water pressure at the end of the construction in Fig. 9 can be used to explain why the settlements still increased with the time in Fig. 6. The continuous increase in the settlements might also result from the penetration of the piles and the compression of the soft soil below the pile tips as shown in Fig. 7.

6.4 Lateral displacement

Figure 10 shows the measured and computed lateral displacements at the toe of the embankment after the last-stage embankment load. It is shown that both the measured and computed lateral displacements were within the range of −7 to 5 mm and the numerical results generally captured the trend of the lateral displacements with depth as compared to the measured data. The lateral displacement became small and could be neglected at the depth of 70 m, which is approximately twice the width of the embankment.

7 Parametric study

To further investigate the performance of the PSS railway embankment, three key influence factors were selected for the parametric study including slab thickness, cushion stiffness, and pile stiffness. In the following discussion, the field study is considered as the baseline case, and each influence factor was varied once at a time to investigate its effects. The computed results below are analyzed at the 340th day.

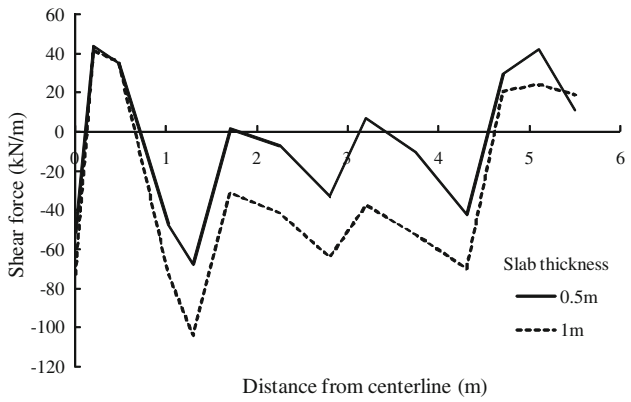

Fig. 11 Influence of the slab thickness on the shear force in the concrete slab

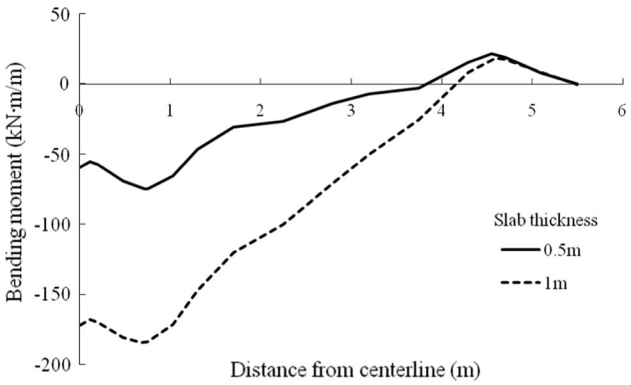

Fig. 12 Influence of the slab thickness on the bending moment in the concrete slab

7.1 Influence of slab thickness

In order to better understand the influence of the slab thickness, the central slab thickness for the numerical analysis was increased from 0.5 m in the baseline case to 1 m. Figures 11 and 12 show the distributions of shear force and bending moment along the central concrete slab at two different slab thicknesses, respectively. It is shown that the shear force and bending moment in the concrete slab both increased with an increase in the slab thickness. The increase in the slab thickness by 2 times increased the maximum shear force and the maximum bending moment in the slab by 55 and 145 %, respectively. The valleys in Fig. 11 correspond to the locations of the piles. Figure 12 shows that the maximum bending moment was close to the centerline of the embankment and the negative moment indicates tension developed at the bottom of the slab. In addition, the increase in the slab thickness slightly reduced the differential settlement of the central slab but had no influence on the settlement and lateral displacement of the embankment (the data are omitted because of limited effect and space).

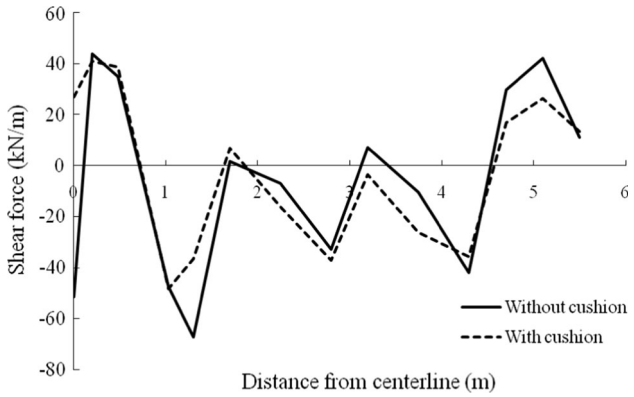

Fig. 13 Influence of the cushion on the shear force in the concrete slab

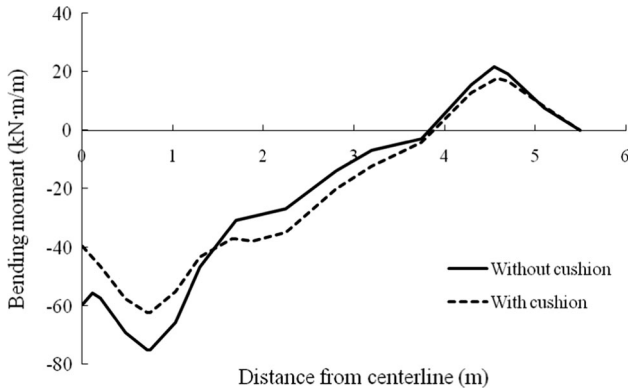

Fig. 14 Influence of the cushion on the bending moment in the concrete slab

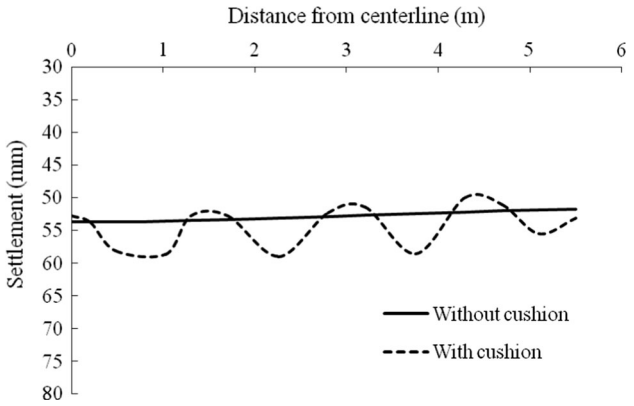

Fig. 15 Influence of the cushion on the differential settlement of on the top of piles under the central slab

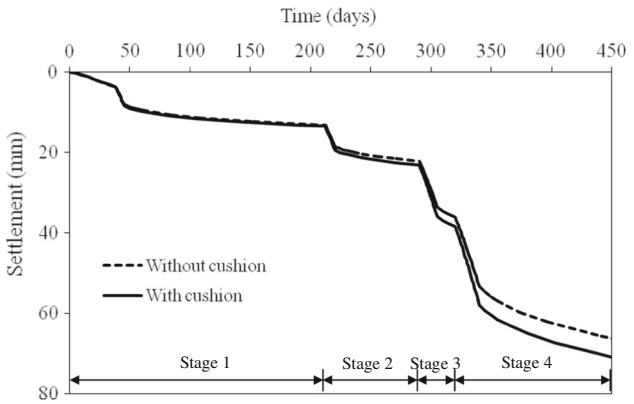

Fig. 16 Influence of the cushion on the maximum settlement at the base of the embankment near the centerline

7.2 Influence of cushion

In China, a granular cushion is often placed between a concrete slab and pile heads to reduce stress concentration on piles and utilize soil resistance between piles. In this study, another model was built with a 0.3-m cushion layer placed below the slab and the pile heads to better understand the effect of the cushion. The cushion was modeled as a linearly elastic–perfectly plastic material with the Mohr–Coulomb failure criterion. The properties of the cushion material are the same as those of the granular cushion under the retaining wall foundation as shown in Table 2. Figures 13 and 14 show the influence of the cushion on the shear force and bending moment in the concrete slab, respectively. It is shown that the shear force and bending moment both were higher in the slab without a cushion than those with a cushion. The existence of the cushion reduced the maximum shear force and the maximum bending moment in the slab by 28 and 17 %, respectively. This phenomenon could be explained that the cushion mobilized the soil resistance between the piles and reduced the stress concentration on the piles. Figure 15 shows the influence of the cushion on the differential settlement on the top of piles under the slab. It is shown that the differential settlement between soil and piles under the slab with the cushion was much larger than that without the cushion. This comparison shows that the cushion increased the flexibility of the foundation and let the soil carry more load. Figure 16 shows the maximum settlement at the base of the embankment near the centerline increased with time. The maximum settlement for the slab with the cushion was larger than that without a cushion because of the compressibility of the cushion. In addition, the cushion had an insignificant influence on the lateral displacement of the embankment (the data are not presented herein to save the space).

7.3 Influence of pile stiffness

To investigate the influence of pile stiffness on the settlement of the embankment and the bending moment and shear force on the concrete slab, the pile modulus was reduced from the baseline case to one tenth that of the baseline one. Figures 17 and 18 show the influence of pile

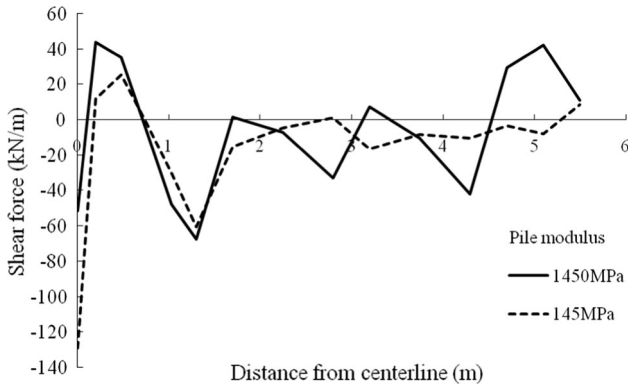

Fig. 17 Influence of pile stiffness on the shear force in the concrete slab

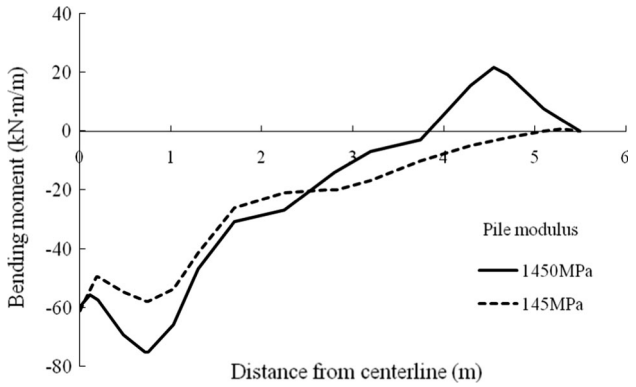

Fig. 18 Influence of pile stiffness on the bending moment in the concrete slab

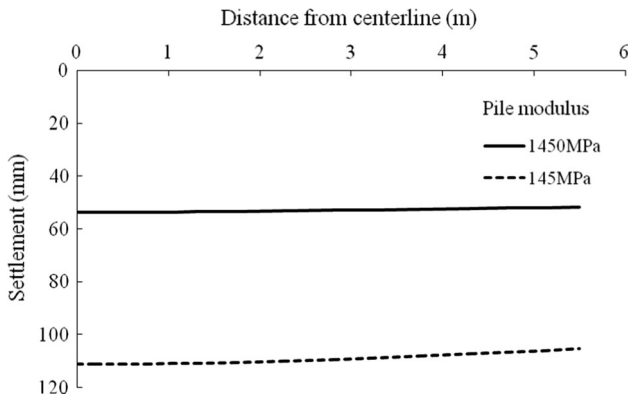

Fig. 19 Influence of the pile stiffness on settlement at the base of the embankment near the centerline

stiffness on the shear force and bending moment in the concrete slab, respectively. It is shown that the shear force and bending moment of slab were both higher when supported by high-stiffness piles than by low-stiffness piles. The pile stiffness by 10 times increased the maximum shear force and the maximum bending moment in the slab by 12 and 30 %, respectively. This phenomenon could be

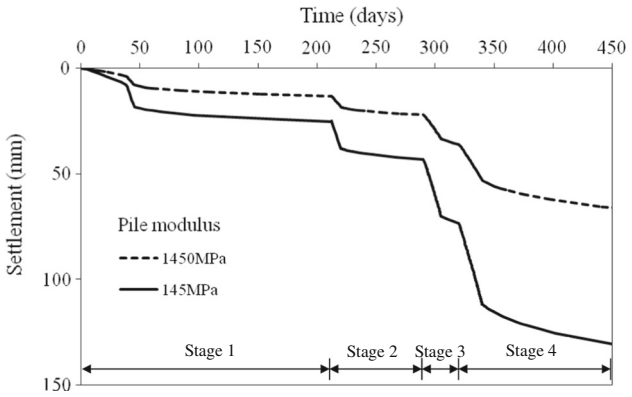

Fig. 20 Influence of pile stiffness on the maximum settlement at the base of the embankment versus time

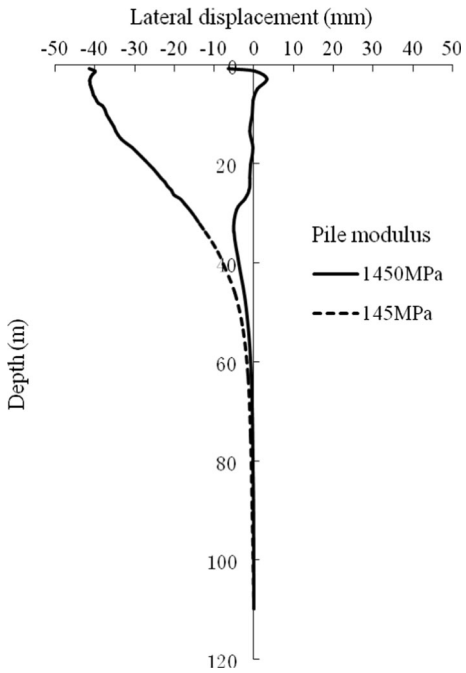

Fig. 21 Influence of pile stiffness on the lateral displacement below the toe of the embankment

explained that the high-stiffness piles could result in the stress concentration on the piles. As expected, a reduction in the pile modulus increased the differential and total settlements as shown in Figs. 19 and 20, respectively. The increase in pile stiffness by 10 times reduced the maximum settlement, differential settlement, and the lateral displacement of the embankment by 50, 67, and 84 %, respectively. Figure 21 shows the influence of the pile stiffness on the lateral displacement below the toe of the embankment. It is shown that the maximum lateral displacement in the embankment on the rigid piles was smaller than that on flexible piles. These results imply that an increase in pile stiffness could reduce the maximum lateral displacement of the embankment.

8 Conclusions

In this study, a field PSS high-speed railway embankment was selected and analyzed using a coupled mechanical and hydraulic numerical model. The numerical results were compared with the field data. A parametric study was conducted to examine three key influence factors. From the comparisons of the numerical results with the field data and in the parametric study, the following conclusions can be drawn:

1. The two-dimensional coupled mechanical and hydraulic model reasonably simulated the performance of the field PSS embankment and the numerical results were compared reasonably well with the field data.
2. Rigid CFG piles carried most of the embankment load. The combination of the rigid piles and the reinforced concrete slab significantly reduced the vertical stresses applied onto the soils between piles.
3. During the construction, the excess pore water pressure in the soil within the top one-third of the pile-treated zone was smaller than that near the tips of the piles.
4. The parametric study showed that the existence of the cushion reduced the maximum shear force and the maximum bending moment in the slab by 28 and 17 %, respectively. The increase in the slab thickness by 2 times increased the maximum shear force and the maximum bending moment in the slab by 55 and 145 %, respectively. The increase in the pile stiffness by 10 times increased the maximum shear force and the maximum bending moment in the slab by 12 and 30 %, respectively.
5. The increase in the pile stiffness by 10 times reduced the maximum settlement, differential settlement, and the lateral displacement of the embankment by 50, 67, and 84 %, respectively.

Acknowledgments This research project was financially supported by the Natural Science Foundation of China (No. 50678115) and the Tianjin Natural Science Foundation (No. 07JCZDJC09800). The China Scholarship Council provided 1-year financial support for the first author being a visiting scholar at the University of Kansas, USA. Their support is greatly appreciated.

References

1. Abusharar SW, Zheng JJ, Chen BG (2009) Finite element modeling of the consolidation behavior of multi-column supported road embankment. Comput Geotech 36(4):675–686
2. Alzamora DE, Wayne MH, Han J (2000) Performance of SRW supported by geogrids and jet grout columns. In: Lutenegger AJ, DeGroot DJ (eds) Performance Confirmation of Constructed Geotechnical Facilities, ASCE Geotechnical Special Publication No. 94, pp 456–466
3. Biot MA (1941) General theory of three-dimensional consolidation. J Appl Phys 12:155–164
4. British Standard BS 8006 (1995) Code of practice for strengthened/reinforced soils and other fills. British Standard Institution, London, p 162
5. Bruce DA (2000) An introduction to the deep soil mixing methods as used in geotechnical applications. Publication No. FHWA-RD-99-138, p 135
6. Card GB, Carter GR (1995) Case history of a piled embankment in London's Docklands. Engineering Geology of Construction, Geological Society Engineering Geology Special Publication, 10, pp 79–84
7. Carlsson B (1987) Reinforced soil, principles for calculation. Linköping, Terratema AB (in Swedish)
8. Chen Y-M, Cao WP, Chen RP (2008) An experimental investigation of soil arching within basal reinforced and unreinforced piled embankments. Geotext Geomembr 26(2):164–174
9. Chen RP, Chen YM, Han J, Xu ZZ (2008) A theoretical solution for pile-supported embankments on soft soils under one-dimensional compression. Can Geotech J 45(5):611–623
10. China Academy of Building Research (2002) Technical code for ground treatment of buildings. Chinese Technical Code JGJ 79-2002, Beijing, p 25
11. Collin JG (2007) U.S. State-of-practice for the design of the geosynthetic reinforced load transfer platform in column supported embankments. Proceedings of GeoDenver 2007 (CD), Denver, CO
12. Giroud JP, Bonaparte R, Beech JF, Gross BA (1990) Design of soil layer-geosynthetic systems overlying voids. Geotext Geomembr 9(1):11–50
13. Han J, Akins K (2002) Case studies of geogrid-reinforced and pile-supported earth structures on weak foundation soils. Geotechnical Special Publication No. 116, Deep foundations 2002. In: O'Neill MW, Towsend FC (eds) Proceedings of the international deep foundation congress. ASCE, Orlando, pp 668–679
14. Han J, Bhandari A, Wang F (2012) DEM analysis of stresses and deformations of geogrid-reinforced embankments over piles. Int J Geomech 12(4):340–350
15. Han J, Gabr MA (2002) Numerical analysis of geosynthetic-reinforced and pile supported earth platforms over soft soil. J Geotech Geoenviron Eng 128(1):44–53
16. Han J, Ye SL (2001) A simplified method for computing consolidation rate of stone column reinforced foundations. J Geotech Geoenviron Eng 127(7):597–603
17. Hewlett WJ, Randolph MF (1988) Analysis of piled embankment. Ground Eng 21(3):12–18
18. Hironaka J, Hirai T, Otani J, Watanabe Y (2008) Load transfer mechanism in reinforced embankment on pile elements. In: Otani, Miyata, Mukunoki (eds) New Horizons in Earth Reinforcement. Taylor and Francis Group, London, pp 741–744
19. Huang J, Han J, Collin JG (2005) Geogrid-reinforced pile-supported railway embankments-three dimensional numerical analysis. J Transp Res Board 1936:221–229
20. Huang J, Han J (2010) Two-dimensional coupled hydraulic and mechanical modeling of geosynthetic-reinforced column-supported embankments. Comput Geotech 37:638–648
21. Huang J, Han J (2009) 3D coupled mechanical and hydraulic modeling of a geosynthetic-reinforced deep mixed column-supported embankment. Geotext Geomembr 27:272–280
22. Huang J, Han J, Oztoprak S (2009) Coupled mechanical and hydraulic modeling of geosynthetic-reinforced column-supported embankments. J Geotech Geoenviron Eng 135(8):1011–1021
23. Jenck O, Dias D, Kastner R (2007) Two-dimensional physical and numerical modeling of a pile-supported earth platform over soft soil. J Geotech Geoenviron Eng 133(3):295–305

24. Jenck O, Dias D, Kastner R (2009) Three-dimensional numerical modeling of a piled embankment. Int J Geomech 9(3):102–112
25. Kempfert HG, Göbel C, Alexiew D, Heitz C (2004) German recommendations for reinforced embankments on pile-similar elements. The 3rd European geosynthetics conference. Deutsche GesellschaftfürGeotechnik, Munich, pp 279–284
26. Kulhawy FH, Trautmann CH, Beech JF, O'Rourke TD, McGuire W, Wood WA, Capano C (1983) Transmission line structure foundations for uplift-compression loading. Report No. EL-2870, Electric Power Research Institute, Palo Alto, CA, USA
27. Ladd CC, Foot R, Ishihara K, Poulos HG, Schlosser F (1977) Stress-deformation and strength characteristics. Proceedings of the 9th ICSMFE, vol 2, State-of-the-Art-Paper, pp 421–494
28. Liu HL, Ng CWW, Fei K (2007) Performance of a geogrid-reinforced and pile-supported highway embankment over soft clay: case study. J Geotech Geoenviron Eng 133(12):1483–1493
29. Magnan J (1994) Methods to reduce the settlement of embankments on soft clay: a review. Vertical-horizontal deformations of foundations and embankments. ASCE, New York, pp 77–91
30. Miki H (1997) Design of deep mixing method of stabilization with low improvement ratio. Proceedings of the first seminar on ground improvement in highways, Bangkok, Thailand, August, pp 197–204
31. Roscoe KH, Burland JB (1968) On the generalized stress strain behaviour of wet clay. In: Heyman J, Leckie FA (eds) Engineering plasticity. Cambridge University Press, Cambridge, pp 535–609
32. Russell D, Pierpoint N (1997) An assessment of design methods for piled embankments. Ground Eng 30(10):39–44
33. Smith M, Filz G (2007) Axisymmetric numerical modeling of a unit cell in geosynthetic-reinforced, column-supported embankments. Geosynth Int 14(1):13–22
34. Stewart ME, Filz GM (2005) Influence of clay compressibility on geosynthetic loads for bridging layer for column supported embankments. Geotechnical Special Publication, No. 131, pp 447–460
35. Svano G, Ilstad T, Eiksund G, Want A (2000) Alternative calculation principle for design of piles embankments with base reinforcement. Proceedings of the 4th international conference of ground improvement geosystem, Helsinki, Finnish Geotechnical Society, pp 541–548
36. Tan SA, Tjahyono S, Oo KK (2008) Simplified plane-strain modeling of stone-column reinforced ground. J Geotech Geoenviron Eng 134(2):185–194
37. Terzaghi K, Peck RB, Mesri G (1996) Soil mechanics in engineering practice, 3rd edn. Wiley, New York
38. Wang F, Han J, Miao LC, Bhandari A (2009) Numerical analysis of geosynthetic-bridged and drilled shaft-supported embankments over large sinkhole. Geosynth Int J 16(6):408–419
39. Zanziger H, Gartung E (2002) Performance of a geogrid reinforced railway embankment on piles. Proceedings of the 7th international conference on geosynthetics, Nice, Balkema, pp 381–386
40. Zheng G, Jiang Y, Han J (2011) Performance of cement-fly ash-gravel pile-supported high-speed railway embankments over soft marine clay. J Mar Georesour Geotechnol 29(2):145–161